Exploring Forest Ecosystem Dynamics using Multivariate Time Series Analysis

Cameron F. T. Pope

University of Aberdeen

MSc Data Science

Student Number 52315403

Full code repository and notebooks can be found on my Github

Data used is open source and can be found here courtesy of the Station for Measuring Ecosystem-Atmospheric Relations (SMEAR)

Abstract

Human induced climate change is disrupting the very fragile balance within ecosystems on which much of life on Earth relies on for survival - a prospect only set to increase in severity along with rising carbon dioxide (CO_2) concentration in the atmosphere with the combustion of fossil fuels, deforestation, and agriculture being the primary contributors[1]. Current projections suggest CO_2 concentration is set to reach 450 parts per million (ppm) by 2040[2], and a worst-case 'business as usual' projection of 910 ppm by 2100[3]. Due to its greenhouse properties, increasing levels of CO_2 in the atmosphere has led to a rise in global temperature of around 1.35°C since 1850[4], with global efforts to limit this to 2.0°C as part of the legally binding Paris Agreement signed by 196 parties at the UN Climate Change Conference (COP21) in Paris, France, in December 2015[5].

Forests play an integral part in meeting this target by regulating atmospheric conditions and mitigating the effects of climate change, with each tree absorbing approximately 25 kilograms of CO_2 per year[6], while producing 28% of the world's oxygen[7]. As such, understanding how our forests react to these changing atmospheric conditions is of extreme importance in allowing more targeted action, both locally in conservation projects, and globally for driving effective political action to protect these ecosystems. The better we understand how climate change is affecting these systems, the more effective the policies can become, the more global leaders will be forced to react in the face of more convincing modeling, and the more research in this area can be conducted. This paper considers the strong modeling and predictive capabilities of deep neural networks (DNNs) in order to understand the effects of climate change on Gross Primary Productivity (GPP) using two decades of hourly data from a state-of-the-art boreal forest monitoring station in Hyytiälä, Finland.

1. Introduction

Forests play an integral part of regulating both local and global climatic conditions. Their ability to absorb carbon dioxide and produce oxygen, provide relief for wildlife, and intercepting precipitation leading to a reduction in surface runoff, increasing lag-time and the severity of the resulting surge[8]. Accounting for 30% of total land area[9], understanding the deep and intrinsic links that these forest ecosystems affect - and are affected by - the wider atmosphere need to be understood to drive global political policy, conservation efforts, and further research. Currently, these links between global

atmospheric conditions and the ecosystems at a local level are still not well understood due to their inherent complexity and the chaotic, non-linear nature of climatic conditions[10], which affects the confidence with which we can make accurate long-term models and predictions[11].

In order to measure a model against our underlying question on how climate change is affecting these forest ecosystems, we need to be able to quantify the productivity of such systems. In this research we use Gross Primary Productivity (GPP) which is defined as the "total amount of carbon compounds produced by photosynthesis of plants in an ecosystem in a given period of time"[12]. Essentially, this equates to the amount of new biomass added to the system as a result of photosynthesis.

Given its reliance on photosynthesis, GPP is significantly lower during nighttime and winter periods, especially in the northern boreal forests in which the SMEAR-II monitoring station is located, whereby less than 6 hours of daylight per day is observed at the height of winter. Consequently, south of the Arctic Circle where there is at least some level of daylight every day, GPP oscillates with periodities of 24 hours and 1 year, representing the daily and seasonal changes respectively (Figures 1 & 2). This brings a unique challenge in which a model will need to be able to encode these daily and seasonal trends and separate them from any longer term trends caused by the changing climate.

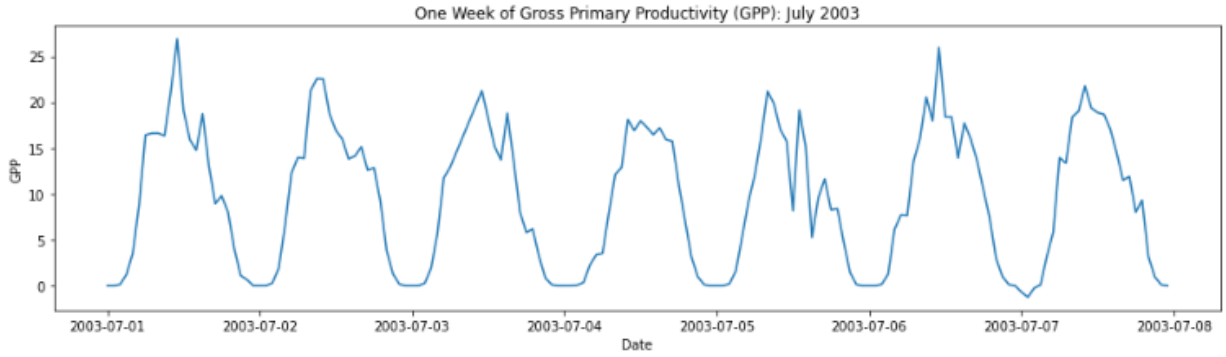

Figure 1: One week of GPP data plotted from the first week of July, 2003

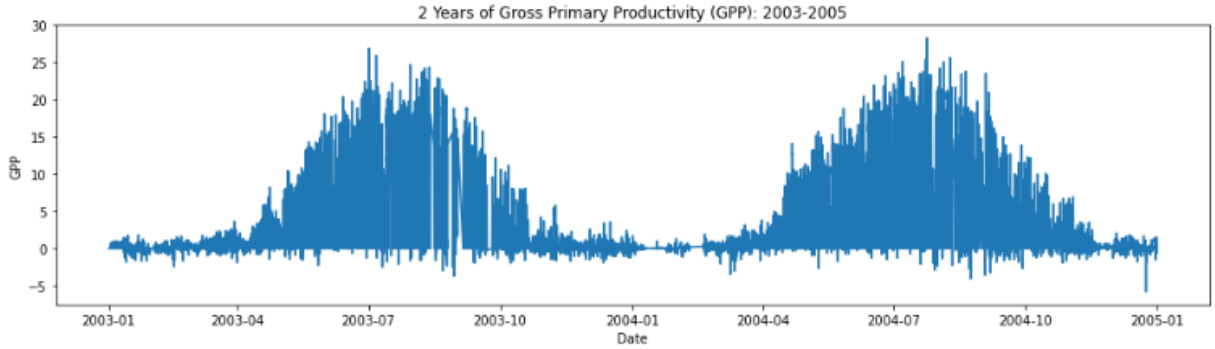

Figure 2: 2 years of GPP data plotted from 2003-2005

The motivation behind the research is to leverage the powerful capabilities of machine learning to further understand how GPP is likely to evolve over time, particularly in light of our rapidly changing climate. The availability and quality of large, open-source datasets and the rise of increasingly effective machine learning methods such as neural networks, combined with far greater computational power has given the possibility to create more accurate predictive models which furthers our understanding in this area, while opening new opportunities for continued research. The fact that these models can be trained, distributed, and run on a modern home PC make this type of project more accessible; decentralizing research which previously has been reserved for supercomputers or clusters with advanced modeling software.

2. Data

2.1 Data

The data was obtained from the station for measuring ecosystem-atmospheric relations (SMEAR) located in Hyytiälä, Finland, 200 kilometers north-west of Helsinki (Figure 3B). It is operated by the University of Helsinki and is the second of such stations, often referred to as SMEAR-II or the SMEAR flagship. It consists of a 128 meter tall measurement mast (Figure 3A) and measurement towers within and above the tree canopy, which continuously monitors forest ecophysiology and productivity, soil and water balance, meteorology, solar and terrestrial radiation, fluxes, ambient concentrations, atmospheric aerosols and deposition[13, 14].

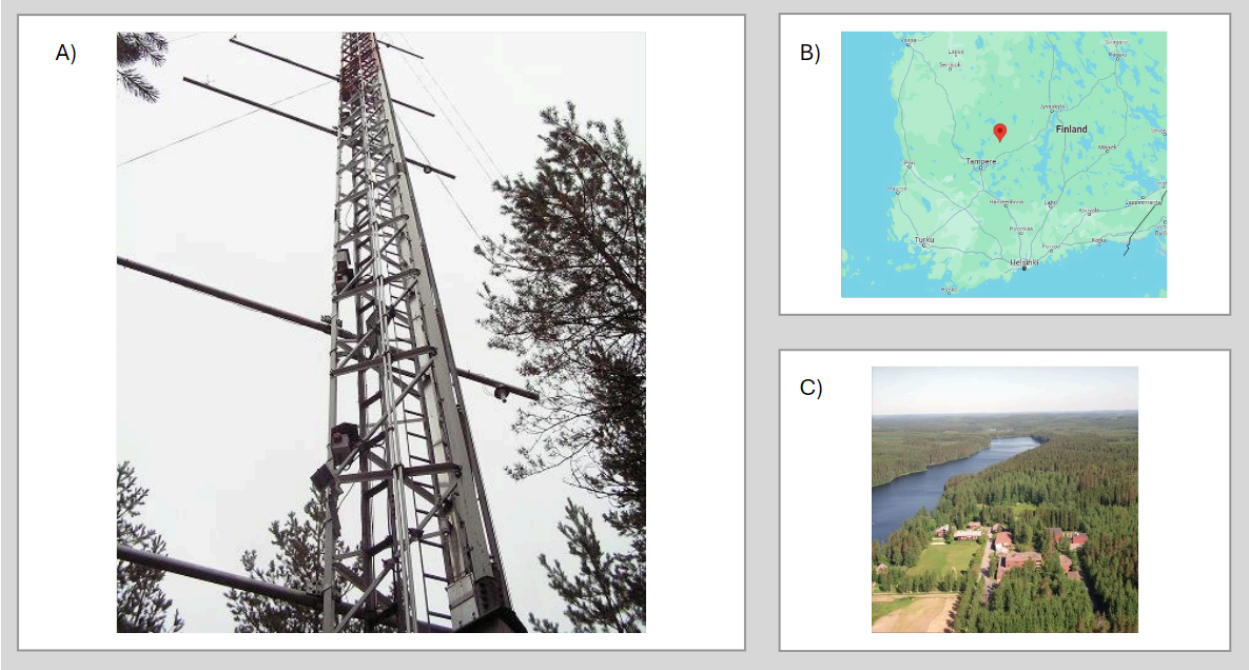

Figure 3: Photo of the 128m tall measurement mast (A), the location of the SMEAR-II facility in Hyytiälä, Finland (B), and an aerial view of the site (C). Images courtesy of SMEAR & the University of Helsinki.

The station is situated in a homogeneous Scots pine boreal forest, the type of which makes up 17% of the Earth's land surface area[15], meaning the results obtained can be interpreted and used as a representation of other, similar, forestland. The station has been operational since 1995 and continuously records over 1200 variables, the majority of which are measured every minute[16]. 20 years of data was obtained from 1 January 2003 to 31 December 2022 with hourly averaging applied to the data using the arithmetic mean. This was done as using a measurement resolution of 1 minute is not only unnecessary when we are considering longer term trends as a result of climate change, but this also has the added benefit of mitigating the effects of noise that would be present with such a granular resolution of data measurement, allowing for a better sense of the overall trend. Throughout the research this averaging window was expanded to 6 and 12 hours to explore the effects this had on the resulting models, which is covered in further detail in section 3.3.

2.2 Feature Selection

When considering the research goal, two further questions needed to be in mind when selecting features to include in the model. Firstly, we needed to identify features which are highly correlated to GPP as this will allow the models to have more statistical power when predicting future values for GPP and

increase the accuracy and confidence of such predictions. Second, we also need features that will be quantifiable in regards to their effect on climate change. For this second question, CO_2 concentration was selected due to being a greenhouse gas representing 79 percent of total greenhouse gas emissions[17], while also playing an important role in photosynthesis whereby carbon compounds are created during respiration. In relation to the first question, air temperature, photosynthetically active radiation (PAR), nitrogen oxide (NO_x) concentration, precipitation, relative humidity, and soil moisture levels were used due to the hypothesis that these features will be sufficient to inform the levels of GPP in the system.

2.3 Data Cleaning

One issue encountered was the reliability of the data, particularly in the earlier years of its operation. For example, 2 years of precipitation data was missing from 2003-2005. Due to no suitable imputation techniques for such a large range of missing data, this feature was discarded. Soil moisture content was also dropped due to its poor correlation with GPP and high proportion of missing data. For other features, methods for filling missing data were possible and had to be decided and reasoned on a case-by-case basis.

For air temperature, missing chunks of data were extremely small in size, typically just a few hours, and as such a spline interpolation of order three was used to find suitable replacements. Spline was chosen due to the sinusoidal structure of air temperature over time. For some other features, they were measured and recorded at various heights above ground level on the primary measurement tower, allowing the combining of multiple series of data into a single series. Relative humidity was one such example, whereby data was downloaded from 2 sensors - one at 16 meters and one at 33 meters above ground level. These two time series were extremely highly correlated with a pearson correlation coefficient of 0.97, meaning we could simply impute missing data from one time series using the observed values from the other, and be confident in the accuracy (Figure 4).

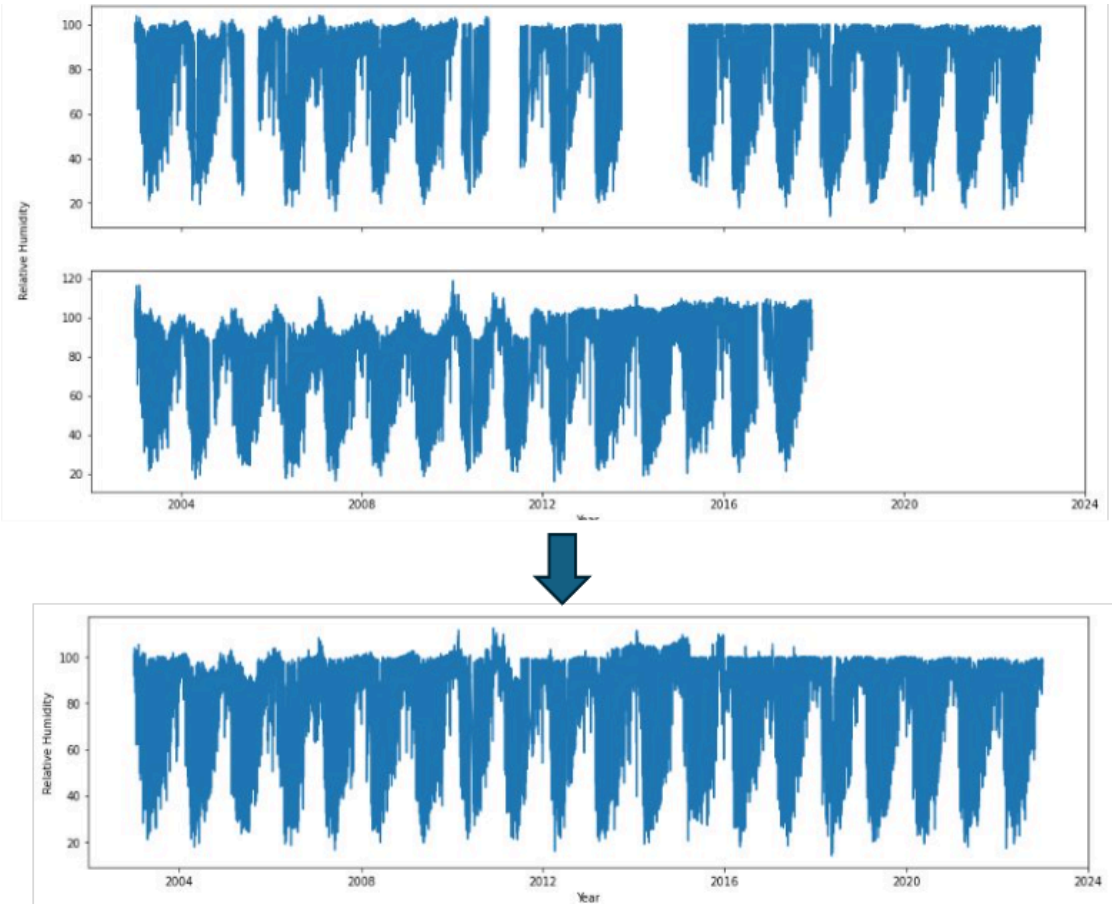

Figure 4: Combining two time series for humidity to create a single series, filling missing values

Due to the limitation of each feature needing to be downloaded separately and only being able to download 10 years data at a time, this resulted in having 22 separate comma separated values (csv) files representing 11 features for our dataset, with each feature being split into two files. A separate script, 'Data Condensing', was created to combine all 22 files into a single csv which we could then import and use in other notebooks.

2.4 Tools

The data cleaning, analysis, visualization, and models were all completed in Python using Jupyter Notebooks[18]. Python is currently the world's most popular programming language according to the TIOBE Index[19] and is used extensively in data science due to its readability, ease of use, and vast selection of libraries capable of streamlining many processes. Jupyter notebooks are a powerful tool in data science due to the ability to show graphs and figures inside the notebook, while also being able to

execute small pieces of code at a time in ‘cells’ with a kernel operating in the background to maintain the current state of variables and defined functions. This ability to run small pieces of code is extremely important in the iterative programming style typically used in data science whereby it is unnecessary to run all of the code whenever we add or test something new. It also allows the ability to add markdown cells which can be extremely useful to create a narrative and ensure technical concepts can be explained to someone in an easy to read way, provide structure to the notebook, as well as adding external links or images.

3. Methods

3.1 Analysis

In order to obtain a preliminary understanding of the dataset, various analysis and visualization techniques were used. This includes methods of quantifying aspects of the dataset such as the mean, maximum and minimum values, and interquartile ranges for each feature. In order to visualize the data, Seaborne’s pairplots produce a grid of scatter plots of each feature pairing allowing an overview of inter-feature relationships, with Pearson correlation heatmaps to quantify and visualize the linear relationships between these features. Due to dealing with time series data with daily and seasonal variation, line plots were created to see how each feature manifests over these time periods. Boxplots were also created based on the data contained within each month of the year (Figure 5) and hour of the day (Figure 6) across the entire 20 year dataset, breaking down the distribution of the dataset across these time periods.

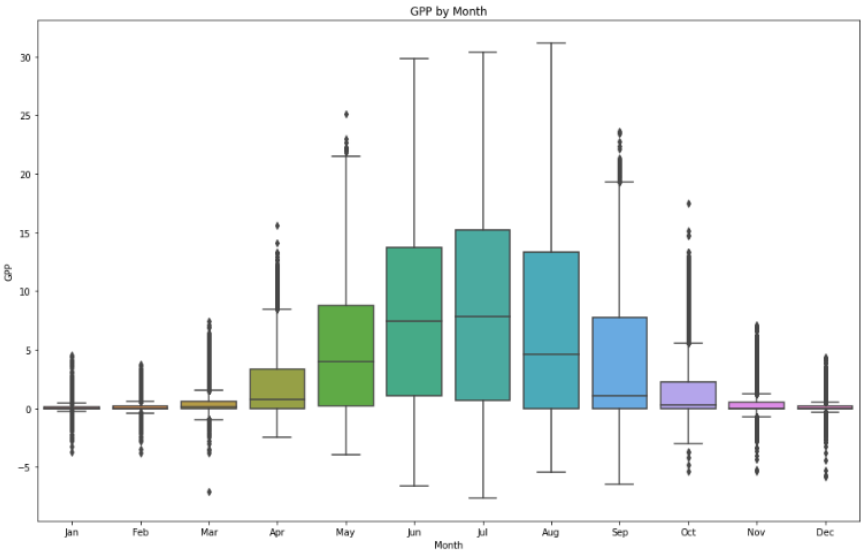

Figure 5: GPP data categorized by month and displayed using a boxplot.

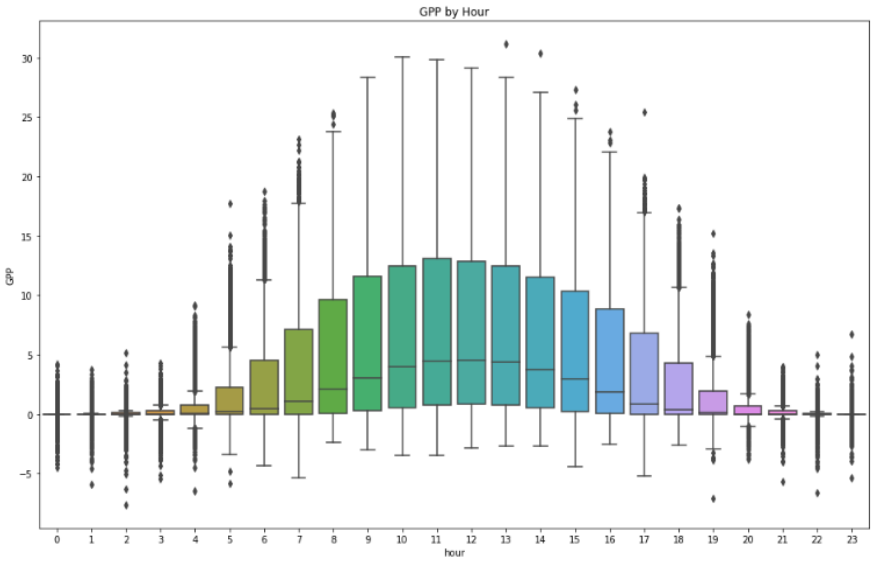

Figure 6: GPP data categorized by hour of the day and displayed using a boxplot.

3.2 Standardization

The data was standardized in preparation for the training of the models. Standardization rescales the data such that the feature mean is reassigned to 0, with a standard deviation of 1. For example, a sample in the dataset which is 2 standard deviations below the mean would become -2 in the rescaled dataset. This is achieved using the formula:

$$X_{stand} = \frac{X - \mu}{\sigma}$$

Whereby μ represents the mean and σ the standard deviation. This has the benefit of ensuring all features are on the same order of magnitude so that one feature does not end up dominating the training process whereby a proportionally smaller change in the value of one feature is assigned a greater significance due to having a greater magnitude of change. Standardization also maintains statistical properties of the dataset such as the spread, while speeding up the convergence of the optimizer and reducing the likelihood of converging on a local - but not global - minima.

3.3 Averaging

In order to determine whether a larger averaging window would have a positive effect on the training of the models, 3 separate datasets were prepared. One of which was the standard 1-hour averaged dataset obtained directly from SMEAR, with an additional 2 datasets created with an averaging window of 6 and 12 hours (Figure 7). This was based on the hypothesis that a larger averaging window further

reduces the noise in the dataset, making the relations between the target and predictor variables easier to learn during the training process. Each of these datasets were then used to train identical models in order to compare their effects on the accuracy of the resulting models. The best performing dataset, chosen based on the lowest Root Mean Squared Error (RMSE) on the testing set, was then used to further optimize the models architecture.

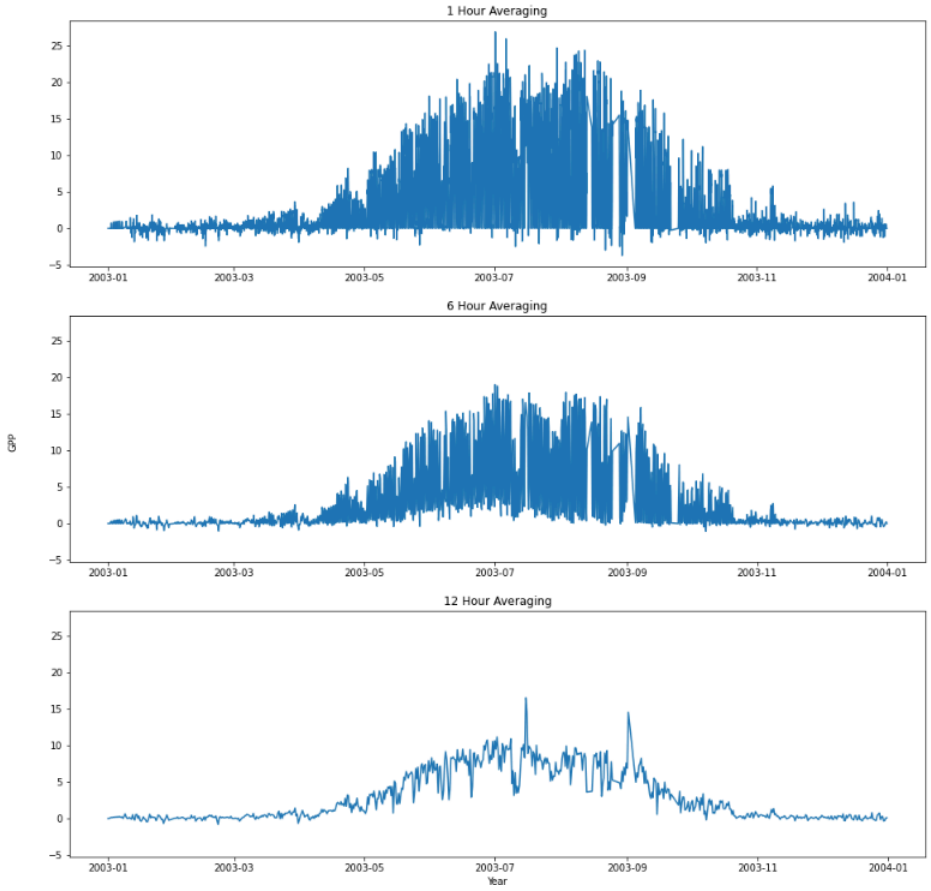

Figure 7: Plots showing the 3 datasets created with 1-Hour, 6-Hour, and 12-Hour averaging for the year 2003

3.4 Structure

Figure 8 shows a summary of the data and models used in the study, and how these were used to create predictions for GPP using feature projections.

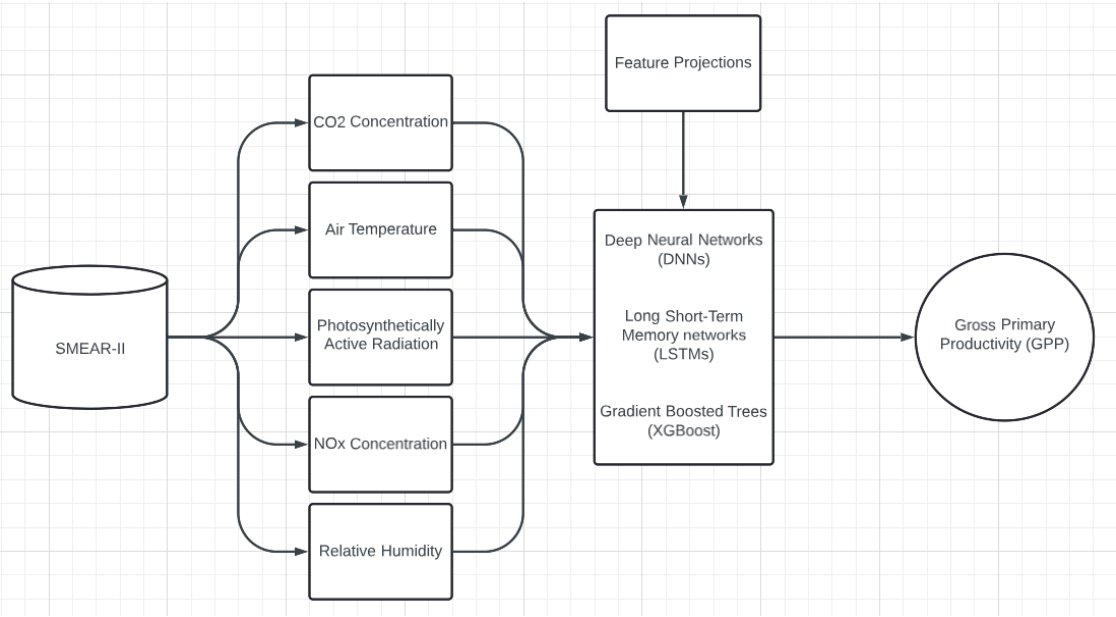

Figure 8: The features and models used and how the data flowed through the project to achieve predictions for GPP.

3.5 Baseline Model

With the rise in popularity of neural networks, including Large Language Models (LLM's) such as OpenAI's ChatGPT, Google's Bard, or Microsoft's Bing AI, it has become a recent trend to throw a neural network at a problem and call it a day, even if it might not be the right tool for the job. With that in mind, a baseline model was created in order to provide a benchmark to measure the neural network against. This allows us to better reason about the true effectiveness of the network, and whether a different machine learning technique would be more suited to this task. For this, a gradient boosting algorithm, XGBoost, was used. This is an ensemble method which combines the output from several, individual decision trees in order to create a single output. Due to having a large number of individual decision trees working towards a majority vote for a prediction, this can help reduce variability and noise of the output. The model utilized 1000 individual decision trees, with the average value across all of these trees used for the overall prediction. XGBoost allows early termination of training if further improvements to the model are not found - in this case after 50 iterations.

3.5 Neural Networks

To create the neural networks, the Keras library was used which acts as an interface for Tensorflow. Throughout the research, a variety of different network architectures were used in

experimentation, including varying number of neurons per layer, number of total layers, including or excluding dropout, different activation layers, learning rates, and replacing the first hidden layer with a Long Short-Term Memory (LSTM) layer which uses the previous n time steps of data in the prediction of a new value, where n is a predetermined window size. From this experimentation, a neural network with 5 hidden layers with rectified linear unit (ReLU) activation functions was settled upon, with 64 neurons in the first hidden layer, decreasing to 4 neurons in the last hidden layer, with a single neuron in the output layer with a linear activation function to allow for negative values. Each dataset with the varying averaging windows was used to train one of these networks in order to identify the best performing set based on this architecture. A second set of networks were also created whereby the first hidden layer was replaced by an LSTM layer with the same number of neurons as the densely connected network and without an activation function, but identical otherwise. A window size of 5 was used, meaning the samples ranging from t - 5 to t - 1 were used in prediction of GPP at time t. Figure 9 demonstrates an example DNN with 3 hidden layers.

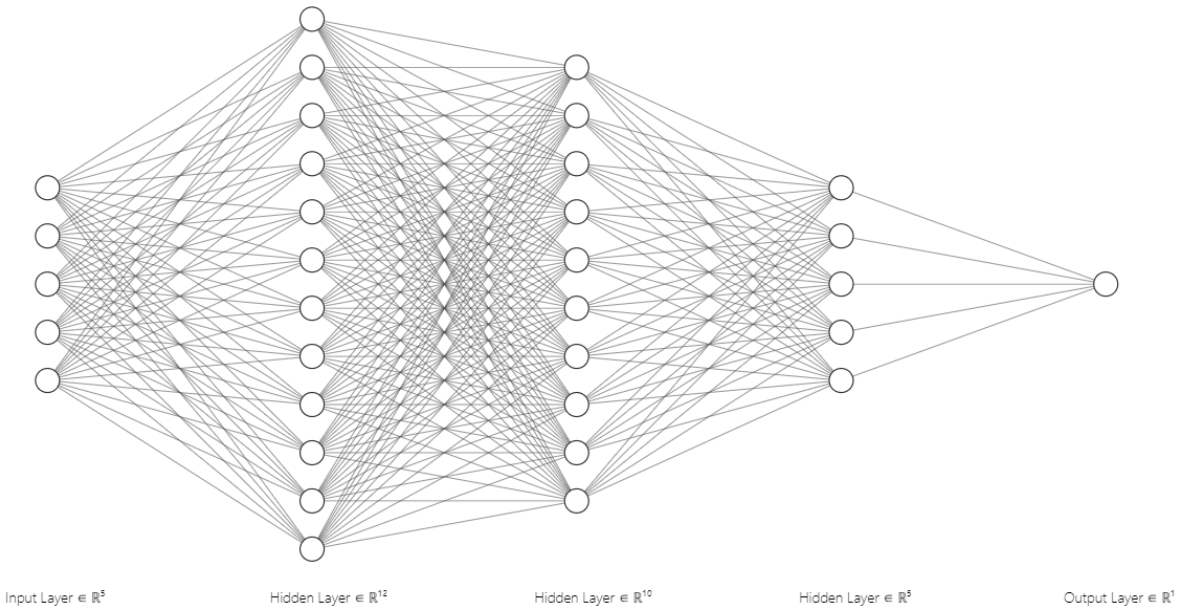

Figure 9: An example DNN with 3 hidden layers with 12, 10, and 5 neurons per layer respectively.
5 neurons on the input layer means 5 predictor features, and 1 neuron on the output layer means a single value prediction.
Created using https://alexlenail.me/NN-SVG/index.html

Resulting from this, a 6-hour window pooled arithmetic mean dataset was selected, with the DNN outperforming the LSTM network. Going from the 1-hour average to a 6-hour average yielded a more effective model due to the further reduction in noise and allowing the model to better learn the relationships between the features and GPP. In order to optimize the model further, Keras Tuner was used which allows random selections of predefined ranges of hyperparameters, evaluating each based on provided objective - in this case the root mean squared error of the model on the validation set. The chosen hyperparameters to search through included a range of neurons per layer varying from 32 to 256 with a step size of 32, a varying number of hidden layers from 1 to 4, a varying amount on dropout after each layer, and a choice from a selection of learning rates from the adaptive momentum (ADAM) optimiser. One hundred different models were built and tested, each with a random selection of hyperparameters from the defined constraints above. The best model can then be saved and used to create new predictions.

3.6 Evaluation

The primary way of evaluating each model was based on the RMSE of the model on the testing set. Due to the squaring of each error, RMSE punishes large errors more heavily than smaller errors. In the case of the XGBoost model, training automatically stopped if no improvements were found after 50 iterations which helps avoid overfitting. For the neural networks, however, the training continues until fully completed based on the parameters we provided when initiating the training. This means we can easily end up overfitting the model, whereby the network begins to memorize the training data and as such loses its ability to generalize, which in turn hurts its performance on new, unseen data. Considering this, the model we end up with at the end of the training process isn’t always at its optimal state. However, we can save the performance metrics of the model after each epoch, allowing us to identify the model's lowest RMSE score and at which epoch this occurred. This is shown in a plot of validation RMSE over the training process (Figure 10). We can also calculate and plot the residuals, which tells us how far each prediction was from the real, observed value (Figure 11), and plot a histogram of the residuals, which gives a sense of the distribution (Figure 12).

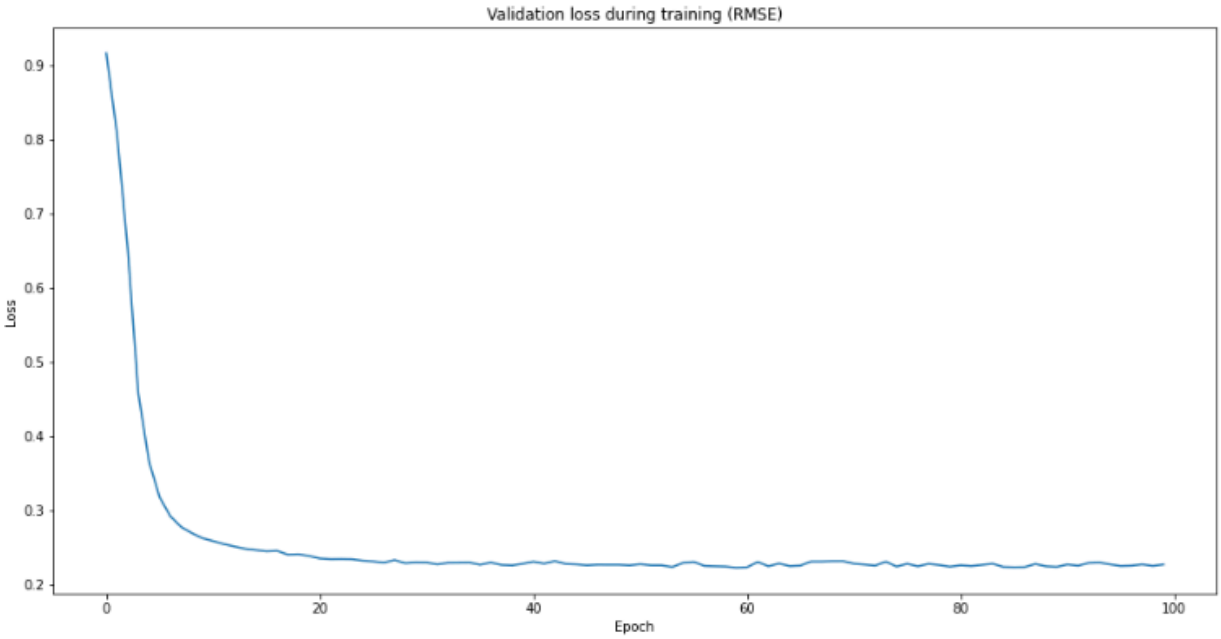

Figure 10: Root mean squared error of the optimized DNN on the validation set after each epoch during the training process

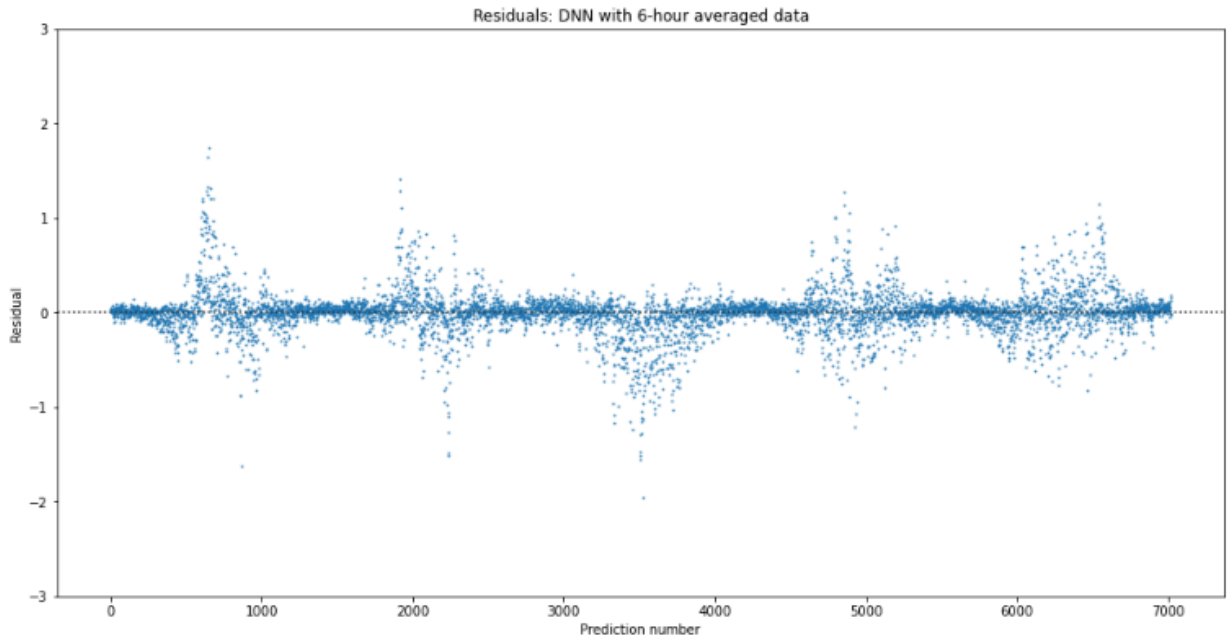

Figure 11: Residual plot of the optimized DNN. A residual of 0 means a perfect prediction.

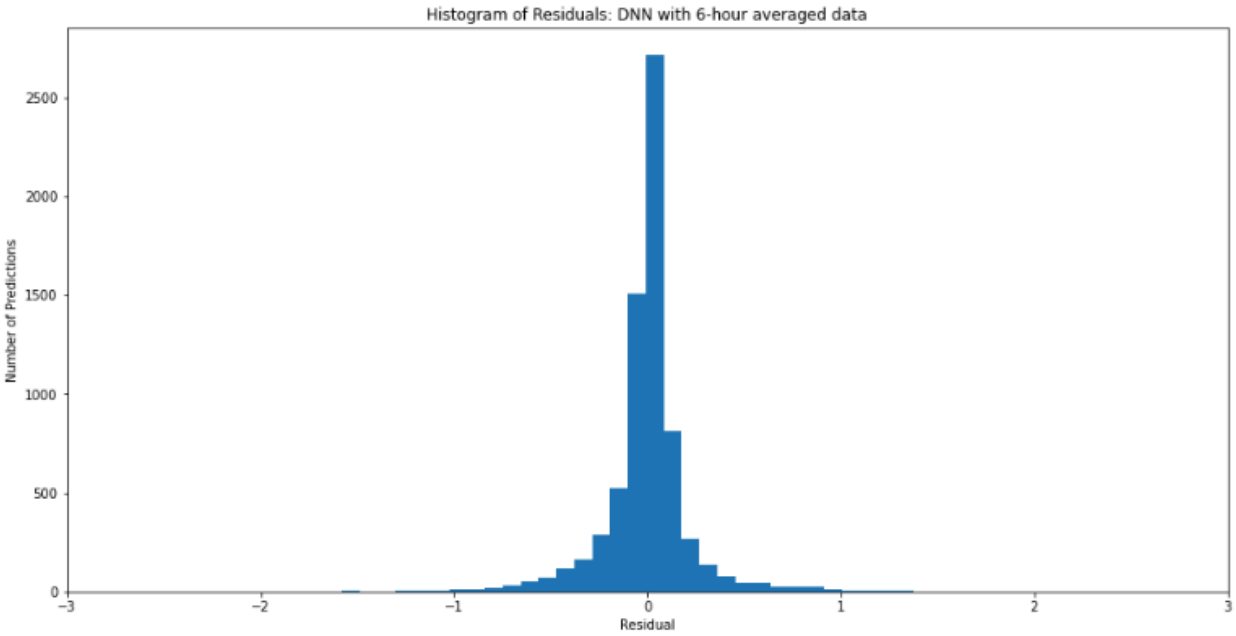

Figure 12: Histogram of residuals of the optimized DNN

4. Main Results

4.1 LSTMs

Somewhat surprisingly, the LSTMs performed rather poorly when compared to regular DNNs. LSTMs rely on using a specified number of previous time steps to inform the prediction of the new value. In the models used, a window size of 5 was used, so a prediction of GPP for time t includes the values of air temperature, CO2 concentration, NOx concentration, humidity, and photosynthetically active radiation from t - 5 to t - 1. Where 1-hour averaging of the data was used, this meant the model would take in the previous 5 hours of data and output a single value of the predicted GPP value. Where 6-hour and 12-hour averaging was used, this window would increase to the previous 30 and 60 hours respectively, albeit encoded within the averaging windows. While this in theory gives a greater depth of information for the model to use to inform a prediction, these models were not able to generalize to the testing set to the same level as the regular DNNs trained on the same dataset. The best performing of the LSTM models was trained on 1-hour averaged, standardized data - achieving an RMSE of approximately 0.34.

The LSTMs performance increased substantially when including previous time steps' GPP values in the training set. This is unsurprising given how GPP from one hour is very strongly correlated with GPP for the next hour. While this model did perform well, the feature importance of such a model means

GPP becomes the dominant feature in predicting the new value for GPP. This would be extremely effective if we were to consider shorter term prediction - for example, using one month's data to predict the following month. This is because we can use known, observed values for GPP in which to inform the model and generate reliable short term projections based on these. However, given the investigation into longer term trends of GPP based on projections for climate change, this is more a question of years and decades, rather than months. While it is theoretically possible to use such a LSTM to predict that far into the future, we are then using the model's predicted values of GPP to inform new predictions. This means a small deviation in initial conditions would lead to vastly different projections, and the confidence in such predictions would rapidly approach zero. This is due to the inherent chaotic nature of atmospheric conditions which drive the levels of GPP in the system.

4.2 Deep Neural Networks (DNNs)

Conversely, while the DNNs technically performed worse than the LSTM including GPP, the model could not simply rely on previous observations of GPP to inform the prediction. The model is instead required to learn the relationships between the rest of the features in order to optimize the RMSE - features of which we have a good understanding of how they are likely to evolve in the coming years. For example, we have a strong understanding of the trend of increasing carbon dioxide concentration in the atmosphere. While there of course remains uncertainty, particularly dependent on how the world's governments respond to continued alarms raised by the scientific community, we can say with a high degree of certainty that the concentration of CO_2 in the atmosphere will continue to rise at a similar level observed in the last two decades. We also understand, save for some cataclysmic shift in conditions such as the North Atlantic Drift breaking down due to continued desalination of the world's oceans as a result of melting freshwater ice[20], that air temperature in this region will also continue to rise at a predictable rate. Essentially, if we are able to create a model that can use features in which we have a high degree of certainty of their future values based on current fossil fuel consumption, the greater the confidence in our predictions we can have. Figure 13 shows a summary of each neural networks performance on the validation set.

	1 Hour	6 Hour	12 Hour	6 Hour Optimized
Dense	0.2868	0.2579	0.3149	0.2508
LSTM	0.3373	0.3753	0.4362	NaN

Figure 13: Table of the performance of each data averaging/model combination. Values are the root mean squared error of observed values compared to predicted values created from the validation data.

The optimized DNN using a 6-hour averaging window on the data still had a tendency to underpredict, particularly in the height of summer where there are large fluctuations between the peaks during the day and the overnight lows, which was exacerbated during years where the GPP peaks were greater than normal, although was able to effectively able to capture the daily and seasonal variations (Figure 14 & 15).

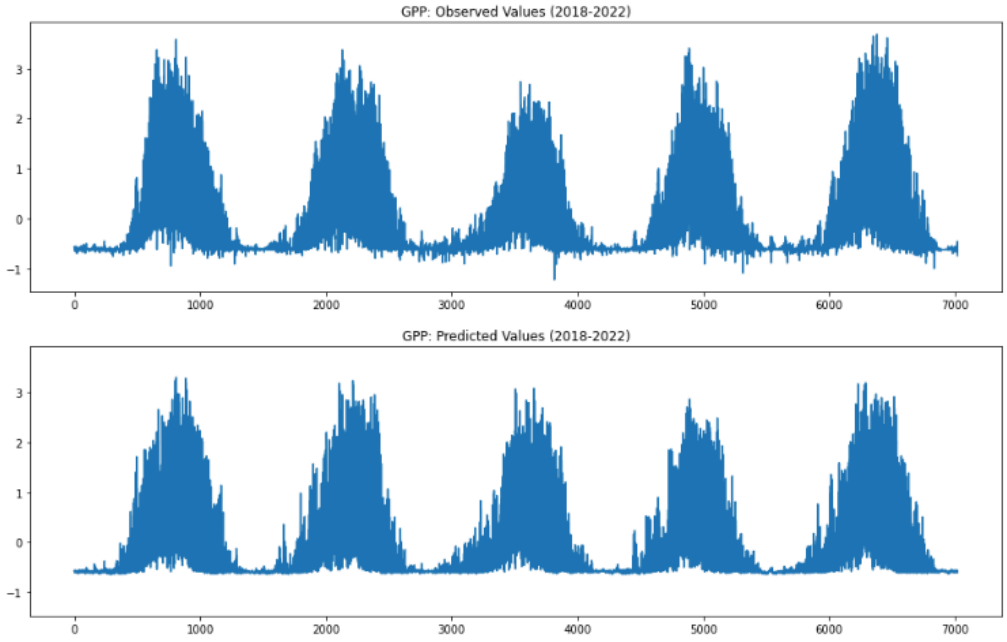

Figure 14: 5 years of observed values for GPP (top) plotted against predicted values for GPP (bottom) using the optimized DNN

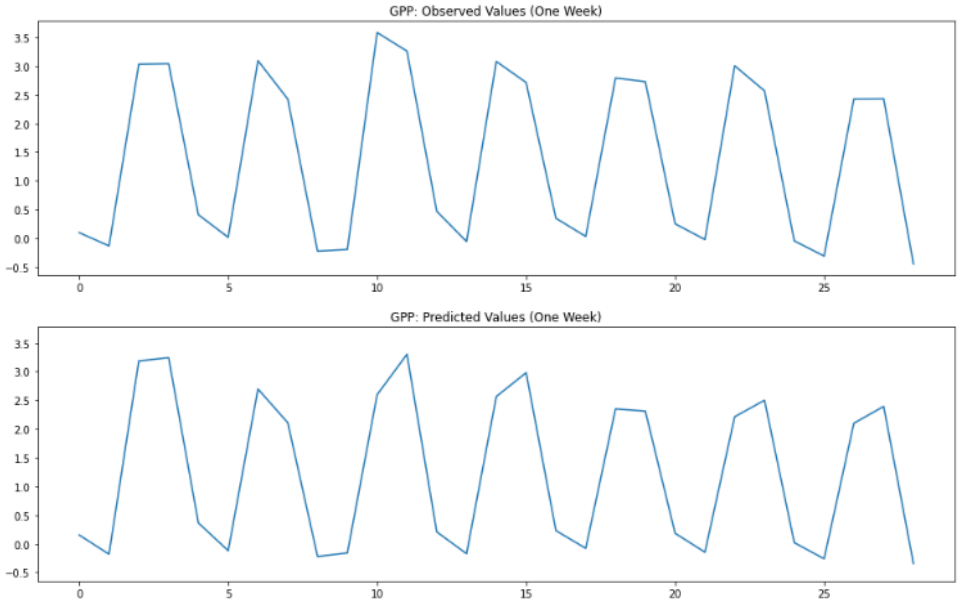

Figure 15: One week of observed values for GPP (top) plotted against predicted values for GPP (bottom) using the optimized DNN

4.3 XGBoost

The XGBoost baseline model did approach the performance of the best neural network, achieving a RMSE of 0.265 when compared to the neural network at 0.250. It was also able to capture the daily and seasonal trends but would tend to overpredict in the spring and autumn, while underpredicting in the summer. It was also less able to correctly model some of the noisier areas of the data, instead opting for smoother seasonal trends.

4.4 Predictions

The best performing model overall was obtained as a result of hyperparameter tuning on the 6-hour averaged DNN, achieving an RMSE of 0.250. This model was subsequently used to generate predictions based on projected figures for CO_2 concentration and air temperature. Predictions were created for the month of July due to this being the time where GPP is at its peak. Data to create the predictions was sampled from a normal distribution, using the mean and standard deviation from observed values during July. For air temperature we created a normal distribution in the same way, but added a constant value of 0.5^{o}C to simulate the warming of the atmosphere. Finally, for CO_2 concentration, NASAs 2040 projection of 450 ppm was used as the mean for the distribution, with a standard deviation

of 15. 100 data samples were generated from these distributions and then fed through the model to create predictions for GPP based on these conditions. A further distribution was created based on observed values of GPP during this same period in order to compare our predictions against.

We can see that the rise in CO_2 and air temperature actually led to a reduction in GPP in both the DNN and XGBoost models (Figure 16), with the XGBoost predicting higher on average, but with a much tighter spread. The models predicting a reduction in GPP is due to the negative correlation between CO_2 concentration and GPP. This is because CO_2 concentration decreases during the summer when GPP is increasing, and increases in the winter when GPP is decreasing. Conducted t-tests found both of these statistically significant, with a p-values of 7.6×10^{-50} for the DNN, and 9.8×10^{-27} for the XGBoost.

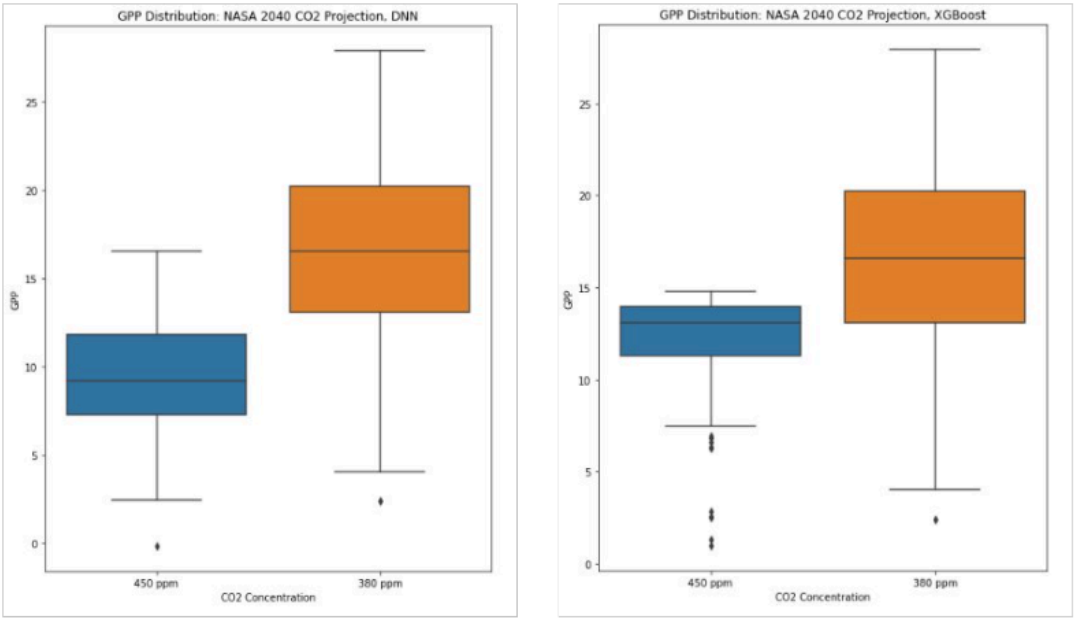

Figure 16: Distribution of GPP predictions based on NASA's 2040 estimate of 450 ppm CO_c concentrations compared to observed values during the same time period. Predictions created from the DNN (Left), and XGBoost (Right) models

5. Discussion

Throughout the research we have successfully created a range of networks capable of modeling both the daily and seasonal trends in GPP, and as a result were able to create predictions for GPP based on existing projections for CO_2 concentration and air temperature. Our findings that the DNNs are best suited to modeling GPP in forests is in alignment to a prior study on the effectiveness of various AI approaches

in the prediction of GPP in the forests of South Korea[21]. Although contrary to acceptance that increasing CO_2 level leads to increased GPP, this project has shown AI is capable at modeling GPP in forests, but further work needs to be done on improving the predictive power of the models

Some key areas for further research would include further optimization of the networks, trialing reservoir computing, and further investigating what drives GPP to include more relevant features into the training process. To correct the negative correlation between CO_2 concentration and GPP due to seasonal variation, a regression component can be added which captures the overall increasing trend in CO_2 concentration.

(Word Count 3997/4000)

6. Acknowledgements

I would like to thank my supervisor for their excellent guidance throughout the project and always being on hand to answer any questions, and for allowing me to take part in a research project that I am passionate about.

References

1. (PDF) F.N. Tubiello, M. Salvatore, R.D. Cóndor Golec, A. Ferrara, S. Rossi, R. Biancalani, S. Federici, H. Jacobs, A. Flammini | Agriculture, Forestry and Other Land Use Emissions by Sources and Removals by Sinks 1990-2011 | Food and Agriculture Organisation (FOA) | https://www.fao.org/3/i3671e/i3671e.pdf
2. Graphic: Cardon Dioxide Hits a New High | NASA | Accessed March 2024 | https://climate.nasa.gov/climate_resources/7/graphic-carbon-dioxide-hits-new-high/
3. Year 2100 Projections | CO2.Earth | Accessed March 2024 | https://www.co2.earth/2100-projections#:~:text=Assuming%20the%20contributions%20are%20made,Celsius%20above%20pre%2Dindutrial%20levels
4. (PDF) Rebecca Lindsey, Luann Dahlman | Climate Change: Global Temperature | National Oceanic and Atmospheric Administration (NOAA) | https://www.energy.gov/sites/default/files/2024-02/093.%20Rebecca%20Lindsey%20and%20Luann%20Dahlman%2C%20NOAA%2C%20Climate%20Change_%20Global%20Temperature.pdf
5. Masson-Delmotte, V., P. Zhai, A. Pirani, S. L. Connors, C. Péan, S. Berger, N. Caud, Y. Chen, L. Goldfarb, M. I. Gomis, M. Huang, K. Leitzell, E. Lonnoy, J.B.R. Matthews, T. K. Maycock, T. Waterfield, O. Yelekçi, R. Yu and B. Zhou (eds.) | IPCC, 2021: Summary for Policymakers. In: Climate Change 2021: The Physical Science Basis. Contribution of Working Group I to the Sixth Assessment Report of the Intergovernmental Panel on Climate Change. Cambridge University Press.
6. How much CO2 does a tree absorb? | Ecotree | Accessed March 2024 | https://ecotree.green/en/how-much-co2-does-a-tree-absorb#answer
7. How Much Oxygen Does a Tree Produce? | Gabrielle Clawson, OneTreePlanted | Accessed March 2024 | https://onetreeplanted.org/blogs/stories/oxygen-tree#:~:text=Except%20instead%20of%20breathing%20in,like%20 phytoplankton%2C%20 producing%20the%20 rest
8. K.R. Chandler, C.J. Stevens, A. Binley, A.M. Keith | Influence of tree species and forest land use on soil hydraulic conductivity and implications for surface runoff generation | DOI: https://doi.org/10.1016/j.geoderma.2017.08.011
9. Seeing Forests for the Trees and the Carbon: Mapping the World's Forests in Three Dimensions | NASA Earth Observatory | Accessed March 2024 | https://earthobservatory.nasa.gov/features/ForestCarbon#:~:text=Forests%20are%20considered%20one%20of,50%20percent%20of%20plant%20productivity.
10. (PDF) B. Moore III, W.L. Gates, L.J. Mata, A. Underdal, R.J. Stouffer, B. Bolin, A. Ramirez Rojas | Advancing our Understanding, IPCC archive | https://archive.ipcc.ch/ipccreports/tar/wg1/pdf/TAR-14.PDF
11. (PDF) Huawei Fan, Junjie Jiang, Chun Zhang, Xingang Wang, Ying-Cheng Lai | Long Term Predictions of Chaotic Systems with Machine Learning | School of Electrical, Computer, and Energy Engineering,

Arizona State University, Tempe, Arizona | DOI: 10.1103/PhysRevResearch.2.012080. https://journals.aps.org/prresearch/pdf/10.1103/PhysRevResearch.2.012080

12. M.S. Ashton et al. (eds.) | Managing Forest Carbon in a Changing Climate | Springer Science + Business Media B.V. 2012 | DOI 10.1007/978-94-007-2232-3
13. Station for Measure Ecosystem-Atmospheric Relations (SMEAR) | University of Helsinki | Accessed March 2024 | https://www.helsinki.fi/en/research-stations/hyytiala-forest-field-station/research/station-for-measuring-ecosystem-atmospere-relations-smear#:~:text=SMEAR%20II%20is%20the%20world's,within%20and%20above%20tree%20canopy.
14. SMEAR-II (Hyytiälä) | Actris National Facility Labeling | Accessed March 2024 | https://actris-nf-labelling.out.ocp.fmi.fi/facility/23
15. Taiga | Juday, Glenn Patrick | *Encyclopedia Britannica*, 19 Sep. 2023 | Accessed March 2024 https://www.britannica.com/science/taiga
16. Markku Kulmala, Anna Lintunen, Ilona Ylivinkka, Janne Mukkala, Rosa Rantanen, Joni Kujansuu, Tuukka Petäjä & Hanna K. Lappalainen - Atmospheric and ecosystem big data providing key contributions in reaching United Nations' Sustainable Development Goals, Big Earth Data, 5:3, 277-305, DOI: 10.1080/20964471.2021.1936943
17. (PDF) Draft Inventory of U.S. Greenhouse Gas Emissions and Sinks: 1990-2022 | United States Environment Protection Agency EPA 430-D-24-001 | Accessed March 2024 | https://www.epa.gov/system/files/documents/2024-02/us-ghg-inventory-2024-main-text.pdf
18. Jupyter Notebooks | https://jupyter.org/
19. TIOBE Index for March 2024 | TIOBE | Accessed March 2024 | https://www.tiobe.com/tiobe-index/
20. Atlantic Circulation Collapse Could Cut British Crop Farming | Phys.org | Accessed March 2024 | https://phys.org/news/2020-01-atlantic-circulation-collapse-british-crop.html
21. Lee B, Kim N, Kim E-S, Jang K, Kang M, Lim J-H, Cho J, Lee Y | An Artificial Intelligence Approach to Predict Gross Primary Productivity in the Forests of South Korea Using Satellite Remote Sensing Data | *Forests*. 2020; 11(9):1000. | https://doi.org/10.3390/f11091000